


Octave-spanning energy-scalable CEP-stabilized pulses from a dual-chirped noncollinear optical parametric amplifier

Zuofei Hong¹  · S. Ali Rezvani² · Qingbin Zhang² · Peixiang Lu^{1,2}

Received: 20 September 2017 / Accepted: 20 October 2017
© Springer Science+Business Media, LLC 2017

Abstract A dual-chirped noncollinear optical parametric amplification scheme exploiting the unique dispersion properties of BiB₃O₆ (BiBO) crystal is proposed. Passively CEP-stabilized 2- μ m pulses from a broadband pumped OPA are efficiently amplified via non-collinear phase-matching in a thin BiBO crystal, resulting in an octave-spanning spectrum that supports a transform limited duration of 10.1 fs. The proposed scheme shows excellent compressibility and high energy scalability for the output signal. Sub-two-cycle CEP-stable mid-IR pulse with energy exceeding 20 mJ can be expected, which is potentially a perfect driving source in attosecond and strong-field researches.

Keywords Dual-chirped optical parametric amplifier · Noncollinear phase-matching · Few-cycle laser pulse

1 Introduction

Intense femtosecond laser pulses have attracted much attention in the past decades for their intriguing prospects in ultrafast optics, strong-field science, graphene plasmonics, and ultrafast spectroscopy (Brabec and Krausz 2000; Krausz and Ivanov 2009; Sansone et al. 2006; Lan et al. 2017; Li et al. 2011, 2017a, b; Qin and Zhu 2017; He et al. 2017; Tong et al. 2017; Ma et al. 2017; Yuan et al. 2017; Long et al. 2017; Wang et al. 2017a, b, c; Ke et al. 2016, 2017; Zhao et al. 2017; Huang et al. 2017; Qin et al. 2016; Liu et al. 2016a, b; Hou et al. 2014, 2016). While the femtosecond technology based on Ti:sapphire or Yb-doped gain medium has been mature and reliable, it can only operate with poor tunability (0.8 μ m for

✉ Qingbin Zhang
zhangqingbin@hust.edu.cn

¹ Laboratory of Optical Information Technology, Wuhan Institute of Technology, Wuhan 430205, China

² School of Physics and Wuhan National Laboratory for Optoelectronics, Huazhong University of Science and Technology, Wuhan 430074, China

Ti:sapphire or 1.04 μm for Yb). Besides, the gain bandwidth in Yb-based system is comparatively narrower, limiting the possibility of producing few-cycle pulses. Compared to such femtosecond laser, longer wavelength light source presents many benefits such as: (1). the ability to generate high energy XUV photonics for imaging and XUV pump-probe applications, (2). the creation of unambiguous tunneling condition at small Keldysh parameters, (3). the extending applications in light-electron interaction and manipulation in solid state. Furthermore, an important feature of pulses with few-cycle durations is the carrier-envelope phase (CEP), which can dramatically affect the electric waveform of the pulse. Therefore, generating few-cycle pulses with high CEP-stability is also in urgent need, especially for application including waveform synthesis (Huang et al. 2011; Manzoni et al. 2012) and strong field ionization (Kübel et al. 2014; Liu et al. 2012).

Due to the outstanding characteristics including broad gain bandwidth, high single-pass gain, high wavelength tunability, and passive CEP stabilization, optical parametric amplification (OPA) has become the most promising source for such pulses. Commercially available Ti:sapphire laser has been widely employed as the pump source in OPA systems. Pumped by the fundamental frequency (FF) of a Ti:sapphire laser, OPA is capable of amplifying pulses from near-infrared (NIR) to mid-infrared (mid-IR) spectral regions (Cerullo and De Silvestri 2003; Brida et al. 2010). Refer to the broad gain bandwidth, noncollinear OPA (NOPA) is an attractive candidate because the group velocity mismatch (GVM) between the signal and idler pulses is compensated through introducing a non-collinear angle. This has been demonstrated in a number of studies in KTiOPO_4 (KTP) (Isaienko and Borguet 2008; Isaienko et al. 2010), KTiOAsO_4 (KTA) (Kraemer et al. 2006), KNbO_3 (KNB) and congruent LiNbO_3 (c-LNB) (Isaienko and Borguet 2013), or periodically poled stoichiometric LiTaO_3 (PPSLT) crystals (Brida et al. 2009; Cirmi et al. 2012), with the pulse energy from μJ to barely mJ level. Yet restricted by the dispersive properties, few examples have been reported using $\beta\text{-BaBO}_3$ (BBO) or BiB_3O_6 (BiBO) crystals, which possess comprehensive advantages such as high effective nonlinear coefficient, high damage threshold, broad transparency range, and inertness to moisture etc. Until lately, Schmidt et al. (2015) proposed a NOPA scheme employing type-II phase-matching in BBO crystal and realized broadband noncollinear phase-matching in the NIR region.

Despite the broadband gain in NIR NOPA systems, the CEP-stabilized idler pulses with longer center wavelengths cannot be directly used because of the angular dispersion originated from the noncollinear geometry. In order to overcome this deficiency, several methods have been proposed. Quasi-phase-matched (QPM) OPA in periodically poled LiNbO_3 (PPLN) crystals seeded by difference frequency generated (DFG) idler can produce CEP-stabilized few-cycle pulses in the mid-IR range (Gu et al. 2009; Deng et al. 2012). Another approach is noncollinear amplification in BBO crystal (Darginavičius et al. 2012), in which the mid-IR seed is also produced in a DFG process (Darginavičius et al. 2012). More recently, Schmidt et al. (2014) proposed the novel frequency-domain OPA (FOPA). The frequency domain is reached via optical Fourier transformation, four different spectral regions are amplified separately and a 1.8- μm 1.4-mJ two-cycle pulse is obtained. Alternatively, a narrowband OPA followed by spectral broadening in hollow core fiber (HCF) has been investigated in many previous researches (Li et al. 2011; Schmidt et al. 2011; Cardin et al. 2015), and the continuum is easily compressed to a sub-two-cycle duration in bulk materials.

Even though the abovementioned systems can generate broadband IR spectra that support few-cycle pulse durations, the energy scalability of the pulses are limited by either the damage threshold or aperture of the used nonlinear crystals and HCF. Moreover, in

some cases, the OPA bandwidth becomes less broad due to the well-known gain narrowing effect if the desired energy gain is too high. On the other hand, the few-cycle IR laser source with several tens mJ energy is essentially of great importance for the energy scaling of high-order harmonics (HH) and isolated attosecond pulses (IAP) (Zhang et al. 2014; Takahashi et al. 2013). As proposed and experimentally investigated in (Zhang et al. 2011; Fu et al. 2015), dual-chirped OPA (DC-OPA) is a promising approach for generating high-energy IR pulses using a Ti:sapphire laser. With the 100-mJ pump pulse, a 1.4-μm uncompressed signal pulse exceeding 20 mJ is produced, and its bandwidth supports a TL duration of 25 fs.

In this paper, we propose and investigate in detail a dual-chirped noncollinear OPA (DC-NOPA) method, which allows us to simultaneously achieve ultrabroadband phase-matching and ultrahigh energy scalability in the mid-IR region, while the CEP stabilization still holds. Taking advantage of broadband gain in BiBO crystal with a small noncollinear angle, an octave-spanning amplified spectrum can be obtained with small distortion in the wavefront. The interacting pulses in the dual-chirped scheme are all temporally stretched, allowing the use of ultrahigh energy pulses while the undesired damage or nonlinear effects are avoided during amplification. The rest of this paper is organized as follows. In Sect. 2, the phase-matching condition in BBO and BiBO crystals are analyzed and compared. In Sect. 3, the concept of BiBO-based DC-NOPA is introduced, the numerical model and system parameters are described. In Sect. 4, the spatial, spectral, temporal properties and the energy scalability of the output signal is investigated. In Sect. 5, the conclusion is drawn and the prospects for high energy mid-IR pulses based on DC-NOPA is discussed.

2 Phase matching in BBO and BiBO crystals

To begin with, we discuss the phase-matching conditions in BBO and BiBO crystals. The gain bandwidth in OPA is determined by the phase-mismatch Δk , which is written as

$$\Delta k = \vec{k}_p - \vec{k}_s - \vec{k}_i,$$

where \vec{k}_m ($m = p, s, \text{ and } i$) stands for the wave vector of the pump, signal, and idler pulses, respectively. The phase-mismatch in collinear geometry can be expanded as

$$\Delta k = \Delta k_0 + \left(\frac{\partial}{\partial \omega} k_i - \frac{\partial}{\partial \omega} k_s \right) \Delta \omega - \frac{1}{2!} \left(\frac{\partial^2}{\partial \omega^2} k_i + \frac{\partial^2}{\partial \omega^2} k_s \right) \Delta \omega^2 + \dots,$$

in which $\Delta k_0 = k_{p0} - k_{s0} - k_{i0}$ is the zero-order phase-mismatch, $\frac{\partial}{\partial \omega} k_i - \frac{\partial}{\partial \omega} k_s$ is the group velocity mismatch between signal and idler pulses (GVM_{si}), and $\frac{\partial^2}{\partial \omega^2} k_i + \frac{\partial^2}{\partial \omega^2} k_s$ is the summation of the group velocity dispersion of the signal and idler pulses (GVD_{si}). The GVM_{si} and GVD_{si} with respect to the signal wavelength in collinear type-I BBO and BiBO crystals are plotted in Fig. 1. The pump wavelength is 0.8 μm.

In collinear OPA, when the signal and idler wavelengths are equal, GVM_{si} is zero, indicating perfect phase-matching to the first order and resulting in a broad gain bandwidth at degeneracy (Brida et al. 2008; Ishii et al. 2012). In this case, Δk is dominated by the second order phase-mismatch GVD_{si}. As observed in Fig. 1b, the minimum absolute values of GVD_{si} are obtained at 1.6 μm in both crystals. It is also noticed that the GVD_{si} in

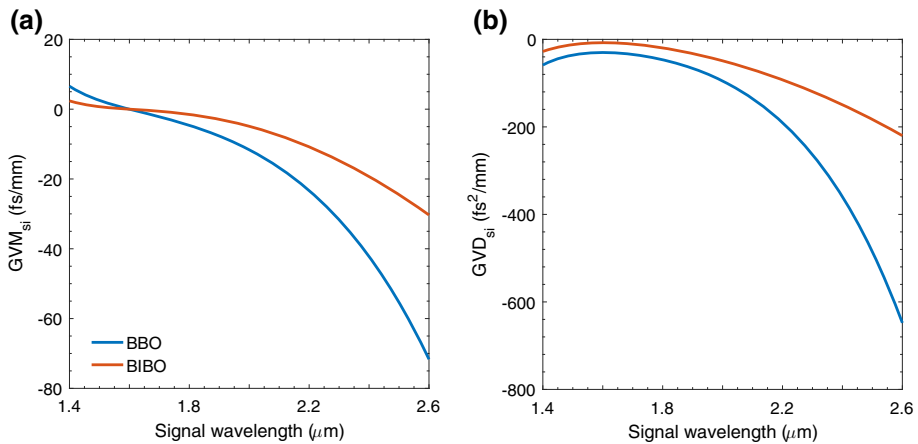


Fig. 1 Group velocity mismatch (a) and group velocity dispersion (b) between signal and idler pulses in type-I BBO (blue lines) and BiBO (red lines) crystals in a collinear geometry. (Color figure online)

BiBO is even more close to zero than in BBO, which results in a broader degenerate gain bandwidth in BiBO crystal (Ishii et al. 2012).

As the signal wavelength shifts away from degeneracy, the first-order phase-mismatch increases with GVM_{si} and the gain bandwidth reduces, thus limiting the wavelength tunability of collinear OPA systems. The idea of NOPA has therefore emerged to compensate GVM_{si} . By introducing a noncollinear angle between the input pump and seed beams, the projection of GV_i is equal to GV_s on the signal propagation direction, allowing phase-matching to the first order.

As widely known, a key condition for noncollinear phase-matching is $GV_s < GV_i$ so the relationship $GV_s = GV_i \times \cos(\Omega)$, Ω being the angle between signal and idler beams, can be met. However, as shown in Fig. 1a, when the signal wavelength is shorter than 1.6 μm , GV_s is larger than GV_i in BBO and BiBO crystals, making it impossible to amplify $< 1.6\text{-}\mu\text{m}$ signal via type-I NOPA designs. This restriction has been recently removed in Schmidt et al. (2015) by using a BBO-based type-II NOPA system, exploiting NIR group velocity matching in a BBO crystal.

In another perspective, even though the gain bandwidth supports a few-cycle duration, the pulse CEP is not stable, adding the difficulty in precisely controlling the electric field or synthesizing of coherent waveforms. It has been proven that the DFG idler between pump and seed pulses from the same source is the most promising candidate for passive CEP-stabilized few-cycle pulses (Baltuska et al. 2002). Using a white light generated (WLG) continuum as the seed, the idler possesses the favorable feature of passive CEP stabilization. The idler pulse is usually centered at $> 1.6\text{-}\mu\text{m}$ wavelength. As shown in Fig. 1a, the $GV_s < GV_i$ relationship is satisfied when the signal wavelength is longer than 1.6 μm . Therefore, if the mid-IR idler in pre amplifier stage is employed as the seed in the following power amplifier stage, noncollinear phase-matching can be realized in BBO and BiBO crystals. Moreover, BiBO is expected to have a better performance in gain bandwidth in a noncollinear geometry, due to its smaller $|GVD_{si}|$ value in this wavelength region.

The detailed noncollinear phase-matching conditions in BBO and BiBO crystals are discussed in Fig. 2. The pump wavelength is fixed at 0.8 μm in all conditions. Figure 2a

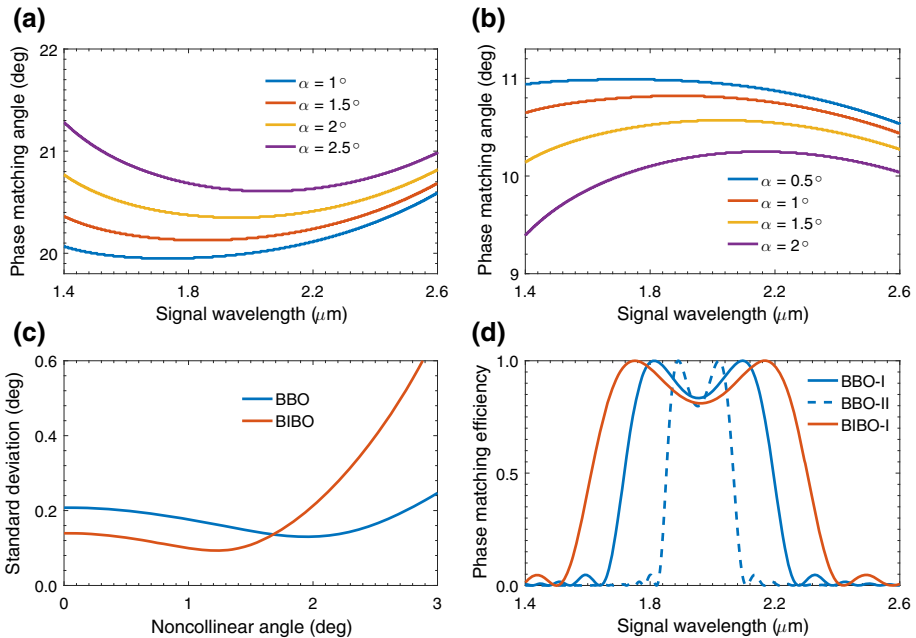


Fig. 2 **a, b** Phase matching curves of BBO and BiBO crystals, respectively, **c** standard deviation of the phase matching curves between 1.4 and 2.6 μm , **d** phase matching efficiency in type-I BBO, type-II BBO and type-I BiBO crystals

and **b** show the noncollinear phase-matching curves in BBO and BiBO crystals, respectively. The group velocity matching points move toward longer wavelength as the noncollinear angle α increases, corresponding to a longer center wavelength for the signal.

The standard deviation (SD) of the phase-matching curves between 1.4 μm and 2.6 μm in Fig. 2a and b are plotted in Fig. 2c. The SD values reveal how flat the phase-matching curve is at different noncollinear angle. The minimal SD point in BiBO crystal (0.09° at $\alpha = 1.3^\circ$) is lower than that in BBO crystal (0.13° at $\alpha = 2.0^\circ$), which indicates a flatter phase-matching curve, hence a broader bandwidth in this spectral region is available. This is also resulted from the lower GVD_{si} in BiBO crystal in a noncollinear geometry.

The phase-matching efficiency $\text{sinc}(\Delta k L / 2)^2$ is also compared in Fig. 2d, Δk is the phase-mismatch regarding different signal wavelength and L is the crystal thickness. The crystal thickness is selected to be 2 mm as an example. In addition, we have discovered that noncollinear type-II phase-matching can be satisfied in this region as well, thus also included in the figure for comparison. The noncollinear angles α and crystal cutting angles θ are 2.0° and 20.4° in type-I BBO, 11° and 56.4° in type-II BBO, 1.3° and 10.7° (xz plane) in type-I BiBO, respectively. It is evidently observed that type-I BiBO crystal has the largest bandwidth around 2 μm compared to type-I and type-II BBO crystals. Moreover, a smaller noncollinear angle leads to less pulse front mismatch between the input beams, which could benefit the beam quality spatially. Therefore, BiBO crystal is an appropriate candidate for noncollinear amplification in the mid-IR range.

3 Concept and model

Based on the above illustrations, we propose a novel DC-NOPA scheme that employs a piece of type-I BiBO crystal for noncollinear amplification of a broadband mid-IR pulse. The schematic setup is depicted in Fig. 3. The system is pumped by a commercially available 0.8- μm /35-fs/1-kHz/7-mJ Ti:sapphire laser. 10% of the laser energy is used to generate the CEP-stabilized broadband idler pulse. This can be realized in our previously proposed broadband pumped OPA system (Rezvani et al. 2017; Hong et al. 2018). The inset in Fig. 3 plots the measured (blue line) and simulated (red line) idler spectra from a broadband pumped OPA. The spectrometer used in the experiment (Ocean Optics NIR-Quest512-2.2) can only measure the spectrum up to 2.2 μm , thus we select the idler centered at 1.7 μm so the majority of the spectrum can be measured. As shown in the figure, a broadband idler spectrum is readily available from the broadband pumped OPA (BBP-OPA) scheme and the calculated result matches well with the experiment, which verifies the validity of the three-dimensional (3D) numerical model used in this paper. In the following investigations, we change the pump-seed delay and the crystal cutting angle in the broadband pumped OPA stage so the center wavelength of idler is shifted to 2 μm .

The idler pulse generated from the BBP-OPA stage is then employed as the seed and amplified in the successive NOPA stage. It is noteworthy that with 0.7 mJ input, the BBP-OPA is capable of producing the broadband idler with higher energy than 10 μJ . However, it is well accepted that a higher energy gain is usually accompanied with gain narrowing effect, therefore a moderate pump energy is selected to obtain a broader bandwidth for the idler pulse. The residual 90% of the laser energy is used to pump the second stage. Both the pump and seed in the second stage are stretched to increase the energy scalability of the system (Zhang et al. 2011; Fu et al. 2015). By stretching the femtosecond pulses to picosecond durations, the interacting pulses can contain much higher energy with a peak intensity still below the damage threshold of the crystal, and the undesired high-intensity-induced nonlinear effects can be prevented. The stretching can be achieved with dispersive components such as a pair of gratings, or with an acousto-optic programmable dispersive filter (AOPDF).

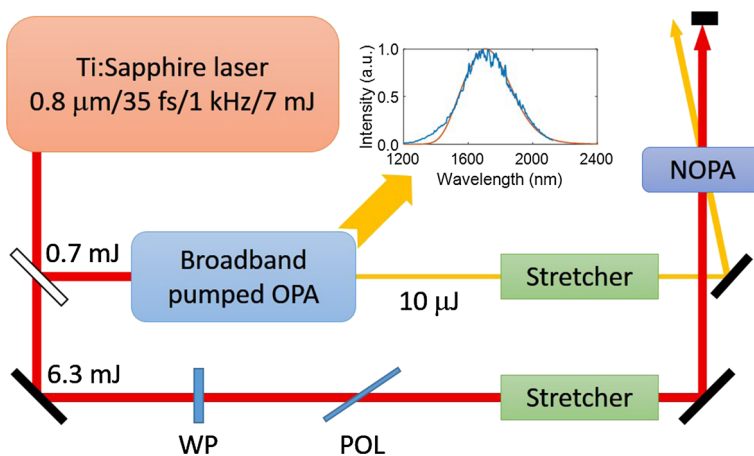


Fig. 3 Schematic setup of BiBO-based DC-NOPA. WP: waveplate, POL: polarizer. Inset: measured (blue line) and calculated (red line) idler spectra from a broadband pumped OPA. (Color figure online)

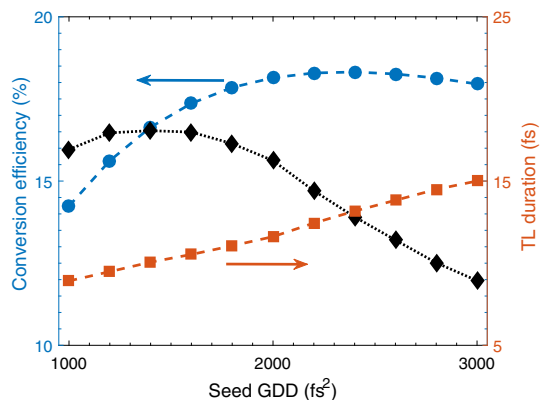
The NOPA process is simulated by numerically solving the coupled-wave equations, in which the diffraction, dispersion up to 4th order, and nonlinear interaction are considered (Zhang et al. 2011; Hong et al. 2014). A 3D model that includes the spatial and spectral/temporal characteristics of the interacting pulses is employed in the simulation. The calculation is done through split-step Fourier transform algorithm, accompanied with 4th order Runge–Kutta numerical method for the nonlinear interaction and Crank–Nicolson method for the diffraction.

The system parameters are as follows. The pump is centered at 0.8 μm , with a transform-limited (TL) duration of 35 fs. The pump pulse is stretched to a duration of 950 fs with a positive GDD of 12,000 fs^2 , the peak intensity after stretching is 14.9 GW/cm^2 , which is around 1/27 of the initial peak intensity. The 10- μJ seed is obtained from the broadband pumped OPA system with a spectrum centered at 2 μm , corresponding to a TL duration of 10.2 fs. Since the ratio of the stretched pump-seed duration affects the performance of the gain bandwidth and conversion efficiency, we vary the seed GDD between 1000 and 3000 fs^2 , corresponding to a stretched pulse duration of 270–820 fs. It is found that the sign of seed GDD is of minor influence on the system performance, therefore only positive seed GDD is investigated. Both the pump and seed beam radii are 3 mm. The crystal cutting angle and noncollinear angle are 10.7° (xz plane) and 1.3° , respectively. The BiBO thickness is selected at 1.5 mm. Note that only 2 mJ of the pump energy is used at beginning, higher pump energies will be used in the later discussion regarding the energy scalability of the system. Since the seed in the second stage already has a pulse energy of 10 μJ , which is only two orders of magnitude lower than the pump, a comparatively thin crystal is sufficient in amplifying the pulse to a high energy.

4 Results

We start the simulation by scanning the GDD of the input seed, as plotted in Fig. 4. The trends of the signal conversion efficiency and TL duration at varying seed GDDs are investigated. As the seed GDD increases, the durations of the stretched pump and seed pulses get closer, and the conversion efficiency is improved owing to a better temporal overlap. On the other hand, when the ratio of the pump-seed duration increases, the signal bandwidth becomes narrower due to the gain narrowing effect, hence the TL duration of the output signal is longer with a larger seed GDD.

Fig. 4 Conversion efficiency (blue circles) and TL duration (red squares) of the output signal with respect to the input seed GDD. Black diamonds indicate the energy bandwidth product (EBP) of the signal pulse. (Color figure online)

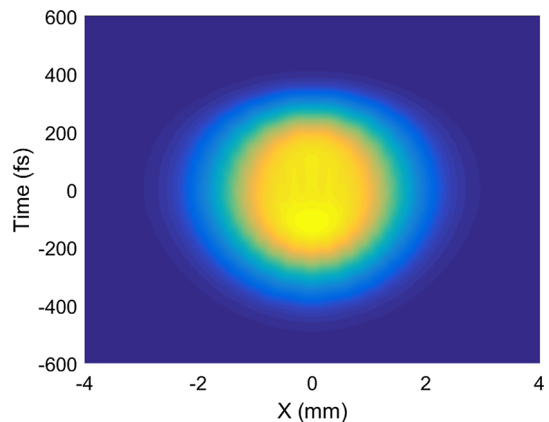


Considering the trade-off between the bandwidth and efficiency during the amplification, we employ the energy bandwidth product (EBP) as a criterion to find out the optimal performance with different seed GDDs, as shown by the black diamonds in Fig. 4. The pulse EBP is the ratio between the pulse energy and the TL duration, which indicates the highest achievable peak power of the pulse. It is found that the maximized EBP is achieved when the seed GDD is 1400 fs^2 , corresponding to a conversion efficiency of 16.6% (the pulse energy is 0.33 mJ) and a TL duration of 10.1 fs for the output signal. Therefore, a seed pulse with the GDD of 1400 fs^2 is applied in the following investigation on the system performances.

The spatial-temporal distribution of the amplified signal is shown in Fig. 5. Even though the noncollinear geometry might introduce spatial distortion into the interacting beams (Giree et al. 2017), it is not observed in the proposed scheme. This is resulted from the small noncollinear angle and the thin BiBO crystal thickness used in the scheme. As discussed in Sect. 2, GVM_{si} in BiBO crystal in a collinear geometry is smaller than that in the BBO crystal, thus a smaller noncollinear angle α is needed, corresponding to less pulse front mismatch between the pump and seed beams. Furthermore, instead of a pJ-level WLG continuum, a μJ -level pulse from a BBP-OPA system is utilized as the seed in the NOPA stage. In this case, the signal can reach saturation within less than 1.5-mm crystal, which also limits the spatial distortion due to the noncollinear geometry. With a noncollinear angle of 1.3° and a crystal of 1.5 mm, the beam shift is 0.03 mm, which is negligible compared to the beam radius of 3 mm. As a result, the amplified signal with good spatial-temporal quality is obtained.

The spectrum and spectral phase of the uncompressed signal are plotted in Fig. 6a, and the input seed (idler from the BBP-OPA stage) spectrum is also included for comparison. As shown by the blue line in Fig. 6a, the output signal spectrum covers 1.4–2.8- μm range with an octave-spanning bandwidth, in which the full width at half maximum (FWHM) bandwidth is even larger than the input spectrum. This is accomplished by slightly detuning the phase-matching angle from the center wavelength. Corresponding to the phase-matching efficiency shown in Fig. 2d, a dent is observed at the center of the spectrum. This specific condition can lead to a broader FWHM bandwidth compared to a perfectly Gaussian-shaped spectrum (Brida et al. 2008). Furthermore, the spectral phase of the amplified signal (red line in Fig. 6a) has a near quadratic shape, corresponding to a linear chirp in the temporal domain. The amplified pulse can therefore be compressed with

Fig. 5 Spatial-temporal profile of the uncompressed output signal



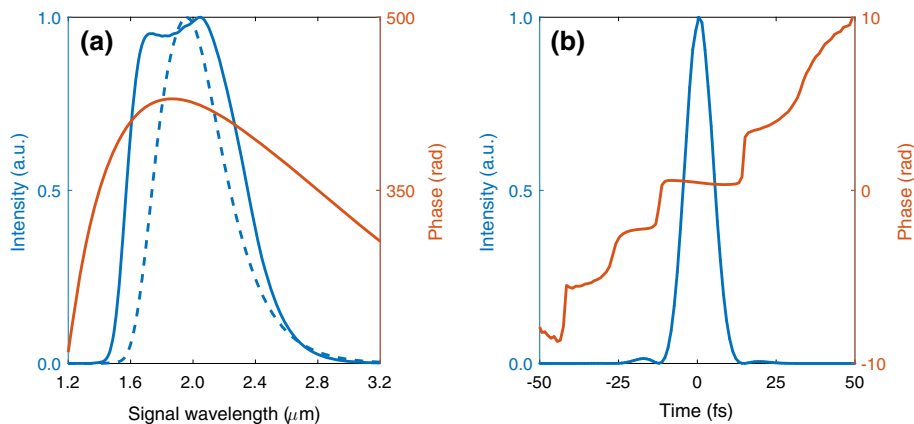


Fig. 6 **a** Spectral profile (blue line) and phase (red line) of the uncompressed signal, blue dashed line is the input seed spectrum, **b** temporal profile (blue line) and phase (red line) of the compressed signal. (Color figure online)

a bulk material such as fused silica. Experimentally speaking, higher order dispersions are inevitable during the stretching and amplification, however, the pre-compensation with an AOPDF is readily available in previous researches (Deng et al. 2012; Ishii et al. 2012), hence the output pulses can be efficiently compressed.

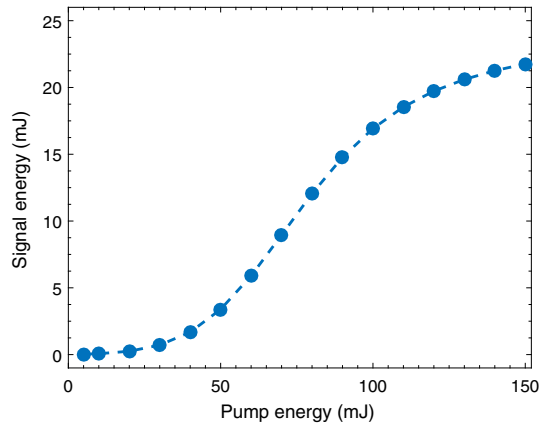
The signal compressibility is confirmed by removing the linear temporal chirp of the output pulse. As mentioned above, the octave-spanning spectrum in Fig. 6a supports a TL duration of 10.1 fs. By introducing a negative GDD of -1400 fs^2 , the signal pulse can be recompressed to a near-TL duration of 10.6 fs, shown by the blue line in Fig. 6b. As revealed by the red line in Fig. 6b, the recompressed signal has a flat temporal phase in the main pulse. Consequently, an efficient compression is achieved by compensating the linear temporal chirp.

According to the above introduction, the main advantage of the dual-chirped scheme is the high energy scalability. With a large temporal chirp introduced to the initial pump, the pulse duration is stretched to several tens or even hundred times longer. With a fixed peak intensity, the chirped pulses contain much higher energy compared to the ultrashort pulses. As a result, hundred-millijoule pulses can be employed in a DC-OPA system.

Next, we investigate the energy scalability of the DC-NOPA system by increasing the pump energy up to 150 mJ. It is found in Fig. 4 that the optimal conversion efficiency is realized when the pump and seed GDDs are 12,000 and 2000 fs^2 , respectively. In order to apply higher pump energy while keep the peak intensity below the damage threshold of BiBO crystal, the GDDs of input pulses are increased proportionally, which are 30,000 and 5000 fs^2 , respectively. Furthermore, the input pump and seed beams are expanded to a radius of 5 mm. This way, the peak intensity of a 150-mJ pump pulse after stretching would be 133.9 GW/cm^2 , which is still lower than the damage threshold of a BiBO crystal (Petrov et al. 2010).

The output signal energy with different pump energy is plotted in Fig. 7. An uncompressed signal with the pulse energy as high as 22 mJ is obtained. A maximum conversion efficiency of 17.0% is achieved when the pump energy is 100 mJ. For pump energies larger than 100 mJ, the upconversion occurs due to saturation. Keep in mind that in the proposed scheme, the signal in NOPA stage (2 μm) has a longer wavelength than the idler

Fig. 7 Signal energy with respect to the pump energy in DC-NOPA system



($\sim 1.33 \mu\text{m}$), more energy is thus transferred to the idler pulse, leading to a lower conversion efficiency for the signal. It is also discovered that with 150-mJ pump energy, the resulted signal spectrum still spans from 1.4 to 2.7 μm , which supports a TL pulse duration of 12.4 fs, revealing the capability of DC-NOPA scheme in producing few-cycle multi-millijoule pulses.

5 Conclusion

In summary, we propose and numerically investigate a novel noncollinear OPA scheme combined with the dual-chirped geometry, in which the ultrabroadband phase-matching and outstanding energy scalability are simultaneously achieved. The noncollinear phase-matching is realized in BiBO crystal, where the group velocity of the long-wavelength mid-IR signal is smaller than the short-wavelength NIR idler. The 2- μm idler pulse from a broadband pumped OPA stage is generated with a pulse energy of 10 μJ and passive CEP-stabilization, which is then utilized as the seed pulse in the successive NOPA stage. Thanks to the μJ -level high-energy seed, a piece of thin BiBO crystal suffices for efficient amplification, which is in favor of both the gain bandwidth and beam quality of the signal pulse. Consequently, an octave-spanning spectrum supporting sub-two-cycle TL duration is obtained, and the output pulse can be compressed to a near-TL duration by compensating the linear temporal chirp. Additionally, the scheme shows high energy scalability owing to the dual-chirped regime while the ultrabroad gain bandwidth is preserved. The non-collinear phase-matching in BiBO crystal provides potential tunability across the mid-IR range by changing the noncollinear angle between the pump and seed beams. We believe that the proposed scheme can markedly benefit the development of various researching fields including attosecond optics and strong-field physics.

Funding This work was supported by the National Natural Science Foundation of China (Nos. 11574101, 11627809).

References

- Baltuska, A., Fuji, T., Kobayashi, T.: Controlling the carrier-envelope phase of ultrashort light pulses with optical parametric amplifiers. *Phys. Rev. Lett.* **88**, 133901 (2002)
- Brabec, T., Krausz, F.: Intense few-cycle laser fields: frontiers of nonlinear optics. *Rev. Mod. Phys.* **72**, 545–591 (2000)
- Brida, D., Cirmi, G., Manzoni, C., Bonora, S., Villoresi, P., De Silvestri, S., Cerullo, G.: Sub-two-cycle light pulses at 1.6 μm from an optical parametric amplifier. *Opt. Lett.* **33**, 741–743 (2008)
- Brida, D., Bonora, S., Manzoni, C., Marangoni, M., Villoresi, P., De Silvestri, S., Cerullo, G.: Generation of 8.5-fs pulses at 1.3 μm for ultrabroadband pump-probe spectroscopy. *Opt. Express* **17**, 12510–12515 (2009)
- Brida, D., Manzoni, C., Cirmi, G., Marangoni, M., Bonora, S., Villoresi, P., De Silvestri, S., Cerullo, G.: Few-optical-cycle pulses tunable from the visible to the mid-infrared by optical parametric amplifiers. *J. Opt.* **12**, 013001 (2010)
- Cardin, V., Thiré, N., Beaulieu, S., Wanie, V., Légaré, F., Schmidt, B.E.: 0.42 TW 2-cycle pulses at 1.8 μm via hollow-core fiber compression. *Appl. Phys. Lett.* **107**, 181101 (2015)
- Cerullo, G., De Silvestri, S.: Ultrafast optical parametric amplifiers. *Rev. Sci. Instrum.* **74**, 1–18 (2003)
- Cirmi, G., Brida, D., Manzoni, C., Marangoni, M., De Silvestri, S., Cerullo, G.: Few-optical-cycle pulses in the near-infrared from a noncollinear optical parametric amplifier. *Opt. Lett.* **32**, 2396–2398 (2012)
- Darginavičius, J., Garejev, N., Dubietis, A.: Generation of carrier-envelope phase-stable two optical-cycle pulses at 2 μm from a noncollinear beta-barium borate optical parametric amplifier. *Opt. Lett.* **37**, 4805–4807 (2012a)
- Darginavičius, J., Tamošauskas, G., Piskarskas, A., Valiulis, G., Dubietis, A.: Generation of tunable few optical-cycle pulses by visible-to-infrared frequency conversion. *Appl. Phys. B* **108**, 1–7 (2012b)
- Deng, Y., Schwarz, A., Fattahi, H., Ueffing, M., Gu, X., Ossiander, M., Metzger, T., Pervak, V., Ishizuki, H., Taira, T., Kobayashi, T., Marcus, G., Krausz, F., Kienberger, R., Karpowicz, N.: Carrier-envelope-phase-stable, 1.2 mJ, 1.5 cycle laser pulses at 2.1 μm . *Opt. Lett.* **37**, 4973–4975 (2012)
- Fu, Y., Takahashi, E.J., Midorikawa, K.: High-energy infrared femtosecond pulses generated by dual-chirped optical parametric amplification. *Opt. Lett.* **40**, 5082–5085 (2015)
- Giree, A., Mero, M., Arisholm, G., Vrakking, M.J.J., Furch, F.J.: Numerical study of spatiotemporal distortions in noncollinear optical parametric chirped-pulse amplifiers. *Opt. Express* **25**, 3104–3121 (2017)
- Gu, X., Marcus, G., Deng, Y., Metzger, T., Teisset, C., Ishii, N., Fuji, T., Baltuska, A., Butkus, R., Pervak, V., Ishizuki, H., Taira, T., Kobayashi, T., Kienberger, R., Krausz, F.: Generation of carrier-envelope-phase-stable 2-cycle 740- μJ pulses at 2.1- μm carrier wavelength. *Opt. Express* **17**, 62–69 (2009)
- He, M., Zhou, Y., Li, Y., Li, M., Lu, P.: Revealing the target structure information encoded in strong-field photoelectron hologram. *Opt. Quant. Electron.* **49**, 232 (2017)
- Hong, Z., Zhang, Q., Lan, P., Lu, P.: Generation of few-cycle infrared pulses from a degenerate dual-pump OPCPA. *Opt. Express* **22**, 5544–5557 (2014)
- Hong, Z., Zhang, Q., Rezvani, S.A., Lan, P., Lu, P.: Tunable few-cycle pulses from a dual-chirped optical parametric amplifier pumped by broadband laser. *Opt. Laser Technol.* **98**, 169–177 (2018)
- Hou, M., Wang, Y., Liu, S.: Sensitivity-enhanced pressure sensor with hollow-core photonic crystal fiber. *J. Lightwave Technol.* **32**, 4035–4039 (2014)
- Hou, M., Wang, Y., Liu, S., Li, Z., Lu, P.: Multi-components interferometer based on partially filled dual-core photonic crystal fiber for temperature and strain sensing. *IEEE Sens. J.* **16**, 6192–6196 (2016)
- Huang, S.-W., Cirmi, G., Moses, J., Hong, K.-H., Bhardwaj, S., Birge, J.R., Chen, L.-J., Li, E., Eggleton, B.J., Cerullo, G., Kärtner, F.X.: High-energy pulse synthesis with sub-cycle waveform control for strong-field physics. *Nat. Photon.* **5**, 475–479 (2011)
- Huang, H., Ke, S., Wang, B., Long, H., Wang, K., Lu, P.: Numerical study on plasmonic absorption enhancement by a rippled graphene sheet. *J. Lightwave Technol.* **35**, 320–324 (2017)
- Isaienko, O., Borguet, E.: Generation of ultra-broadband pulses in the near-IR by non-collinear optical parametric amplification in potassium titanyl phosphate. *Opt. Express* **16**, 3949–3954 (2008)
- Isaienko, O., Borguet, E.: Ultrabroadband few-cycle infrared pulse generation from a noncollinear optical parametric amplifier based on bulk niobate crystals. *J. Opt. Soc. Am. B* **30**, 2075–2080 (2013)
- Isaienko, O., Borguet, E., Vöhringer, P.: High-repetition-rate near-infrared noncollinear ultrabroadband optical parametric amplification in KTiOPO_4 . *Opt. Lett.* **35**, 2834–2832 (2010)
- Ishii, N., Kaneshima, K., Kitano, K., Kanai, T., Watanabe, S., Itatani, J.: Sub-two-cycle, carrier-envelope phase-stable, intense optical pulses at 1.6 μm from a BiB_3O_6 optical parametric chirped-pulse amplifier. *Opt. Lett.* **37**, 4182–4184 (2012)

- Ke, S., Wang, B., Qin, C., Long, H., Wang, K., Lu, P.: Exceptional points and asymmetric mode switching in plasmonic waveguides. *J. Lightwave Technol.* **34**, 5258–5262 (2016)
- Ke, S., Wang, B., Long, H., Wang, K., Lu, P.: Topological mode switching in a graphene doublet with exceptional points. *Opt. Quant. Electron.* **49**, 224 (2017)
- Kraemer, D., Hua, R., Cowan, M.L., Franjic, K., Dwayne, R.J.: Miller, Ultrafast noncollinear optical parametric chirped pulse amplification in KTiOAsO₄. *Opt. Lett.* **31**, 981–983 (2006)
- Krausz, F., Ivanov, M.: Attosecond physics. *Rev. Mod. Phys.* **81**, 163–234 (2009)
- Kübel, M., Alnaser, A.S., Bergues, B., Pischke, T., Schmidt, J., Deng, Y., Jendrzewski, C., Ullrich, J., Paulus, G.G., Azzeer, A.M., Kleineberg, U., Moshhammer, R., Kling, M.F.: Strong-field control of the dissociative ionization of N₂O with near-single-cycle pulses. *New J. Phys.* **16**, 065017 (2014)
- Lan, P., Ruhmann, M., He, L., Zhai, C., Wang, F., Zhu, X., Zhang, Q., Zhou, Y., Li, M., Lein, M., Lu, P.: Attosecond probing of nuclear dynamics with trajectory-resolved high-harmonic spectroscopy. *Phys. Rev. Lett.* **119**, 033201 (2017)
- Li, Y., Chen, W., Wang, H., Liu, N., Lu, P.: Bragg gratings in all-solid Bragg photonic crystal fiber written with femtosecond pulses. *J. Lightwave Technol.* **29**, 3367–3371 (2011a)
- Li, C., Wang, D., Song, L., Liu, J., Liu, P., Xu, C., Leng, Y., Li, R., Xu, Z.: Generation of carrier-envelope phase stabilized intense 1.5 cycle pulses at 1.75 μm . *Opt. Express* **19**, 6783–6789 (2011b)
- Li, Y., Li, M., Zhou, Y., Ma, X., Xie, H., Lan, P., Lu, P.: Carrier-envelope phase dependent photoelectron energy spectra in low intensity regime. *Opt. Express* **25**, 11233–11243 (2017a)
- Li, L., Wang, Z., Li, F., Long, H.: Efficient generation of highly elliptically polarized attosecond pulses. *Opt. Quant. Electron.* **49**, 73 (2017b)
- Liu, K., Zhang, Q., Lu, P.: Enhancing electron localization in molecular dissociation by two-color mid-and near-infrared laser fields. *Phys. Rev. A* **86**, 033410 (2012)
- Liu, S., Wang, Z., Hou, M., Tian, J., Xia, J.: Asymmetrically infiltrated twin core photonic crystal fiber for dual-parameter sensing. *Opt. Laser Technol.* **82**, 53–56 (2016a)
- Liu, S., Tian, J., Liu, N., Xia, J., Lu, P.: Temperature insensitive liquid level sensor based on antiresonant reflecting guidance in silica tube. *J. Lightwave Technol.* **34**, 5239–5243 (2016b)
- Long, H., Bao, L., Habeeb, A.A., Lu, P.: Effects of doping concentration on the surface plasmonic resonances and optical nonlinearities in AGZO nano-triangle arrays. *Opt. Quant. Electron.* **49**, 345 (2017)
- Ma, X., Li, M., Zhou, Y., Lu, P.: Nonsequential double ionization of Xe by mid-infrared laser pulses. *Opt. Quant. Electron.* **49**, 170 (2017)
- Manzoni, C., Huang, S.-W., Cirimi, G., Farinello, P., Moses, J., Kärtner, F.X., Cerullo, G.: Coherent synthesis of ultra-broadband optical parametric amplifiers. *Opt. Lett.* **37**, 1880–1882 (2012)
- Petrov, V., Ghotbi, M., Kokabee, O., Esteban-Martin, A., Noack, F., Gaydardzhiev, A., Nikolov, I., Tzankov, P., Buchvarov, I., Miyata, K., Majchrowski, A., Kityk, I.V., Rotermund, F., Michalski, E., Ebrahim-Zadeh, M.: Femtosecond nonlinear frequency conversion based on BiB₃O₆. *Laser Photon. Rev.* **4**, 53–98 (2010)
- Qin, C., Wang, B., Long, H., Wang, K., Lu, P.: Nonreciprocal phase shift and mode modulation in dynamic graphene waveguides. *J. Lightwave Technol.* **34**, 3877–3883 (2016)
- Qin, M., Zhu, X.: Molecular orbital imaging for partially aligned molecules. *Opt. Laser Technol.* **87**, 79–86 (2017)
- Rezvani, S.A., Hong, Z., Pang, X., Wu, S., Zhang, Q., Lu, P.: Ultrabroadband tunable OPA design using spectrally broadened pump source. *Opt. Lett.* **42**, 3367–3370 (2017)
- Sansone, G., Benedetti, E., Calegari, F., Vozzi, C., Avaldi, L., Flammini, R., Poletto, L., Villoresi, P., Altucci, C., Velotta, R., Stagira, S., De Silvestri, S., Nisoli, M.: Isolated single-cycle attosecond pulses. *Science* **314**, 443–446 (2006)
- Schmidt, B.E., Shiner, A.D., Lassonde, P., Kieffer, J.-C., Corkum, P.B., Villeneuve, D.M., Légaré, F.: CEP stable 1.6 cycle laser pulses at 1.8 μm . *Opt. Express* **19**, 6858–6864 (2011)
- Schmidt, B.E., Thiré, N., Boivin, M., Laramee, A., Poitras, F., Lebrun, G., Ozaki, T., Ibrahim, H., Légaré, F.: Frequency domain optical parametric amplification. *Nat. Commun.* **5**, 3643 (2014)
- Schmidt, C., Bühler, J., Heinrich, A.-C., Leitenstorfer, A., Brida, D.: Noncollinear parametric amplification in the near-infrared based on type-II phase matching. *J. Opt.* **17**, 094003 (2015)
- Takahashi, E.J., Lan, P., Mücke, O.D., Nabekawa, Y., Midorikawa, K.: Attosecond nonlinear optics using gigawatt-scale isolated attosecond pulses. *Nat. Commun.* **4**, 2691 (2013)
- Tong, A., Zhou, Y., Lu, P.: Bifurcation of ion momentum distributions in sequential double ionization by elliptically polarized laser pulses. *Opt. Quant. Electron.* **49**, 77 (2017)
- Wang, S., Wang, B., Qin, C., Wang, K., Long, H., Lu, P.: Rabi oscillations of optical modes in a waveguide with dynamic modulation. *Opt. Quant. Electron.* **49**, 389 (2017a)
- Wang, Z., Wang, B., Long, H., Wang, K., Lu, P.: Surface plasmonic lattice solitons in semi-infinite graphene sheet arrays. *J. Lightwave Technol.* **35**, 2960–2965 (2017b)

- Wang, F., Qin, C., Wang, B., Long, H., Wang, K., Lu, P.: Rabi oscillations of plasmonic supermodes in graphene multilayer arrays. *IEEE J. Sel. Top. Quant. Electron.* **23**, 125–129 (2017c)
- Yuan, H., Li, F., Long, H.: Control of high-order harmonic generation with chirped inhomogeneous fields. *J. Opt. Soc. Am. B.* **34**, 2390–2395 (2017)
- Zhang, Q., Takahashi, E.J., Mucke, O.D., Lu, P., Midorikawa, K.: Dual-chirped optical parametric amplification for generating few hundred mJ infrared pulses. *Opt. Express* **19**, 7190–7212 (2011)
- Zhang, Q., He, L., Lan, P., Lu, P.: Shaped multi-cycle two-color laser field for generating an intense isolated XUV pulse toward 100 attoseconds. *Opt. Express* **22**, 13213–13233 (2014)
- Zhao, D., Wang, Z., Long, H., Wang, K., Wang, B., Lu, P.: Optical bistability in defective photonic multilayers doped by graphene. *Opt. Quant. Electron.* **49**, 163 (2017)